Erbium in crystal silicon: Optical activation, excitation, and concentration limits

A. Polman, G. N. van den Hoven, J. S. Custer,[a] J. H. Shin, and R. Serna
FOM-Institute for Atomic and Molecular Physics, Kruislaan 407, 1098 SJ Amsterdam, The Netherlands

P. F. A. Alkemade
DIMES/CST, Delft University of Technology, Lorentzweg 1, 2628 CJ Delft, The Netherlands

(Received 14 July 1994; accepted for publication 18 October 1994)

The optical activation, excitation, and concentration limits of erbium in crystal Si are studied. Preamorphized surface layers of Czochralski-grown (Cz) Si(100), containing 1.7×10^{18} O/cm^3, were implanted with 250 keV Er at fluences in the range 8×10^{11}–8×10^{14} cm^{-2}. After thermal solid-phase epitaxy of the Er-doped amorphous layers at 600 °C, Er is trapped in the crystal at concentrations ranging from 3×10^{16} to 7×10^{19} Er/cm^3, as measured by secondary-ion-mass spectrometry. Photoluminescence spectra taken at 77 K show the characteristic Er^{3+} intra-4f luminescence at 1.54 μm. Photoluminescence excitation spectroscopy shows that Er is excited through a photocarrier-mediated process. Rapid thermal annealing at 1000 °C for 15 s increases the luminescence intensity, mainly due to an increase in minority-carrier lifetime, which enhances the excitation efficiency. Luminescent Er forms clusters with oxygen: the maximum Er concentration that can be optically activated is determined by the O content, and is $(3\pm1)\times10^{17}$ Er/cm^3 in Cz-Si. The internal quantum efficiency for electrical excitation of Er in Cz-Si is larger than 3×10^{-6}.

I. INTRODUCTION

Erbium doping of silicon has recently become an extensively studied subject. The rare earth erbium, when incorporated in Si in the trivalent charge state, shows characteristic luminescence from an intra-4f transition at a wavelength of 1.54 μm. This emission can be observed both under optical or electrical excitation. This optical doping technique seems to be a promising way around the problem of the indirect band gap, which precludes efficient light emission from pure crystal Si. If sufficiently high Er concentrations could be incorporated and activated in crystal Si, it would become possible to fabricate light emitting diodes, lasers, or optical amplifiers, based on silicon. This would enable the integration of optical and electronic technologies on the same chip.

Erbium doping of Si was introduced by Ennen *et al.*, who incorporated Er into crystal Si (c-Si) using Er ion implantation during Si molecular-beam epitaxy.[1,2] Subsequent studies have addressed the enhancement of the Er luminescence efficiency in Si by the addition of impurities,[3,4] the optical[5,6] and electrical[7–9] characteristics of Er in Si, and the structural aspects associated with the incorporation of Er in Si.[10–18] Recent work has focused on the attainment of room-temperature photoluminescence (PL) from Er-doped Si. It was found that the addition of oxygen to Er-doped Si enhances the concentration of luminescent Er, and reduces the quenching of the PL at elevated temperatures.[19] As a result, room-temperature PL from Er and O co-doped Si has been observed. Ion implantation,[3,4,9] chemical-vapor deposition,[20,21] and molecular-beam epitaxy[22] have been used to fabricate such Er and O co-doped samples. Most recently, it was found that Er and O co-doped Si p-n diodes show room-temperature electroluminescence at 1.54 μm.[23–25] However, up to now the luminescence intensities and quantum efficiencies obtained for Er in Si are still quite small.

The attainment of efficient luminescence from Er in Si requires four factors: (1) High concentrations of Er must be incorporated in the crystal; (2) the Er must be incorporated in an optically active (luminescent at 1.54 μm) configuration; (3) the luminescence efficiency (lifetime) must be high; and (4) the Er must be efficiently excited.

In order to improve the emission from Er in Si these fundamental issues all need to be addressed. Recently, we have shown that Er concentrations as high as 2×10^{20} Er/cm^3 can be incorporated into c-Si.[13,18] This was done using high-dose Er implantation into c-Si, which causes amorphization of the implanted surface layer. The Er-doped amorphous (a-Si) layer was then recrystallized using thermal solid-phase epitaxial recrystallization at relatively low temperatures (500–600 °C). During regrowth, Er was segregated at the moving a-Si/c-Si interface and trapped in the growing crystal. The details of the segregation and trapping behavior are described in Ref. 18. The attainment of such high Er concentrations fulfills the first requirement mentioned above.

In this article we address the other three requirements. The annealing characteristics of these highly Er-doped Si films are studied, with the aim to obtain maximum photoluminescence at 1.54 μm. Changes in the Er PL intensity are described in terms of Er active fraction, Er luminescence lifetime, and carrier lifetime in the crystal. Furthermore, measurements are shown of Er PL intensity as a function of Er concentration. It is concluded that the maximum Er concentration that can be optically activated in Czochralski-grown (Cz) Si is $(3\pm1)\times10^{17}$ Er/cm^3. Possible configura-

[a]Present address: Sandia National Labs, M/S 1056, Albuquerque, NM 87185.

 0021-8979/95/77(3)/1256/7/$6.00

tions of Er in Si are discussed, as well as quantum efficiencies for electrical excitation of Er.

II. EXPERIMENT

Ion implantation was performed with a 1 MV Van de Graaff accelerator, using a sputter ion source with an Er metal cathode. All implants were performed with the samples kept at 77 K. Cz-grown (100)Si wafers were used to make two sets of samples. The first set was made by direct Er implantation into Si(100) (n-type, 1–30 Ω cm) at 250 keV to a fluence of 9×10^{14} Er/cm^2. After solid-phase-epitaxial (SPE) recrystallization of the implantation-amorphized surface layer at 600 °C (15 min), 65% of the Er was trapped in the crystal to a maximum concentration of 9×10^{19} cm^{-3}, as measured using Rutherford backscattering spectrometry (RBS).[13,18] Subsequent thermal annealing in the temperature range 600–1300 °C was applied to these samples in a rapid thermal annealing (RTA) furnace under flowing Ar. The second set was made by Er implantation into Cz-Si samples which were first amorphized using a 350 keV, 3×10^{15} Si/cm^2 implant. Erbium was then implanted at 250 keV into the amorphized films at fluences of 8×10^{11}, 8×10^{12}, 8×10^{13}, or 8×10^{14} Er/cm^2. Following the implants, the films were recrystallized at 600 °C (15 min) and subsequently annealed in the RTA at 1000 °C under flowing N_2. After annealing, the Er concentration profiles as a function of depth were determined with secondary-ion-mass spectrometry (SIMS) using 6 keV O_2^+ sputtering. All secondary-ion intensities were converted into atomic densities using known relative sensitivity factors.[26] The O content in the Cz-Si wafers in this study was determined with SIMS using 16 keV Cs^+ sputtering, and was found to be $(1.7\pm0.5)\times10^{18}$ O/cm^3.

PL spectroscopy was performed using the 514.5 nm line of an Ar laser as a pump source. The light beam was focused to a 1-mm-diam spot on the sample. The $1/e$ penetration depth at this wavelength is 890 nm in c-Si.[27] For most measurements the pump power at the sample was fixed at 160 mW. The pump beam was mechanically chopped at 55 Hz. The luminescence signal was collected using a 48 cm monochromator, a liquid-nitrogen-cooled Ge detector, and a lock-in amplifier. The spectral resolution was 6 nm. All PL measurements were performed using a liquid-nitrogen-cooled cryostat, with the samples kept in vacuum (10^{-7} mbar). PL decay measurements were performed using mechanical modulation of the beam. The decay signals were recorded and averaged using a digitizing oscilloscope system. The total system response time was 30 μs. Photoluminescence excitation spectroscopy was performed using a Ti:sapphire laser which was tuned in the wavelength range 925–1030 nm at a fixed pump power of 10 mW at the sample. The Ti:sapphire laser was pumped using all lines of an Ar laser at a power of roughly 5 W.

III. RESULTS AND DISCUSSION

A. Optical activation of Er in Si

1. PL spectra and annealing behavior

Figure 1 shows a PL spectrum (measured at 77 K) of Er-implanted Cz-Si (9×10^{14} Er/cm^2) after SPE at 600 °C.

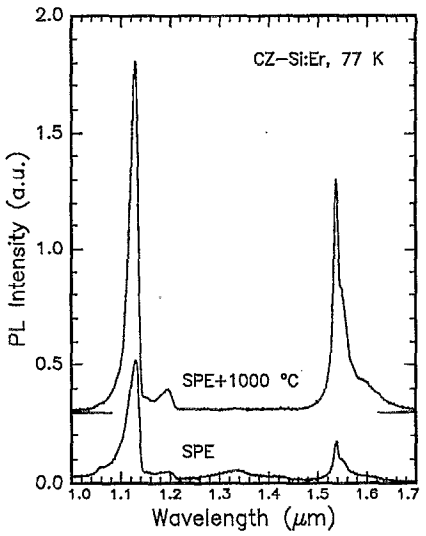

FIG. 1. Photoluminescence spectra taken at 77 K for Er-implanted Si (250 keV, 9×10^{14} cm^{-2}) after SPE recrystallization at 600 °C (lower spectrum), and after subsequent thermal annealing at 1000 °C for 15 s (upper spectrum). The upper spectrum was shifted vertically for clarity. The pump power at 514.5 nm was 160 mW; the resolution 6 nm.

The spectrum shows four clear features around 1.131, 1.20, 1.34, and 1.54 μm, respectively. The first two peaks correspond to phonon-assisted near-band-edge (BE) luminescence of Si.[28] The broad band around 1.3 μm is very similar to defect bands found earlier for ion-damaged Si after annealing.[28] The peak around 1.54 μm represents the characteristic luminescence from Er^{3+} and originates from transitions between the first excited $^4I_{13/2}$ manifold and the $^4I_{15/2}$ ground manifold. A spectrum for the sample regrown by SPE and subsequently annealed at 1000 °C for 15 s is also shown in Fig. 1. As can be seen, the defect band has now disappeared and both the Er and the band-edge luminescence have increased. PL decay measurements were also performed and show a slight nonexponential behavior.[19] The typical $1/e$ time for both samples in Fig. 1 was 0.80 ± 0.05 ms.

The data in Fig. 1 show that the Er PL intensity can be increased fivefold by subsequent thermal annealing at 1000 °C. Anneals were also performed at other temperatures in the range 600–1300 °C (15 s) and it was found that annealing at 1000 °C resulted in the optimum Er PL intensity at 1.54 μm. Figure 2 shows measurements of the Er PL peak intensity at 1.54 μm as a function of annealing time at 1000 °C. The intensity after 0 s annealing corresponds to that of the sample after SPE (bottom curve in Fig. 1). As can be seen the optimum annealing time is 15 s; longer annealing reduces the Er PL intensity. The BE PL intensity at 1.131 μm is also indicated in Fig. 2. It shows a threefold increase after annealing for 15 s and also a decreasing trend for longer annealing times. The Er $1/e$ PL lifetimes are also indicated in the figure. The lifetime increases from 0.75 ± 0.05 ms for the sample after SPE, to 0.98 ± 0.05 ms after subsequent annealing at 1000 °C for 5 min. The lifetime of the BE luminescence was also measured, but could not be resolved within the 30 μm time resolution of the system. Indeed, it is ex-

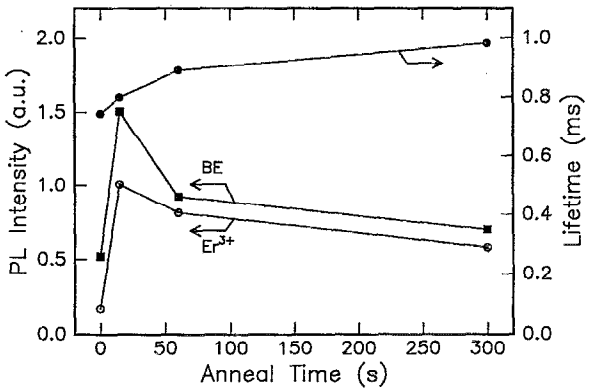

FIG. 2. Measurements at 77 K of the Er PL intensity at 1.54 μm, the BE luminescence at 1.131 μm, and the Er luminescence lifetime at 1.54 μm, all as a function of annealing time at 1000 °C. The samples were implanted with 250 keV Er at 9×10^{14} cm^{-2} and recrystallized by SPE at 600 °C. The pump power at 514.5 nm was 160 mW.

pected that the minority-carrier lifetime in ion implanted and doped crystal Si is much less than 30 μs.

2. Er excitation

Erbium may be excited in Si either by direct absorption or through a photocarrier-mediated process. To distinguish between the two effects, photoluminescence excitation spectroscopy was performed using a Ti:sapphire laser tuned at wavelengths in the range 925–1030 nm. Note that the Si band-gap energy at 77 K corresponds to a wavelength of 1063 nm. Figure 3 shows the 1.535 μm luminescence intensity as a function of pump wavelength for the Er-implanted Cz-Si sample (SPE+1000 °C). The pump power was fixed at 10 mW at each wavelength and the data were taken at 77 K. As can be seen the Er luminescence signal is a slightly monotonically decreasing function of pump wavelength (a small feature is seen at 1003 nm, which is not related to Er, as the PL spectrum taken using this pump wavelength (not shown) does not show the typical spectral shape for Er^{3+}).

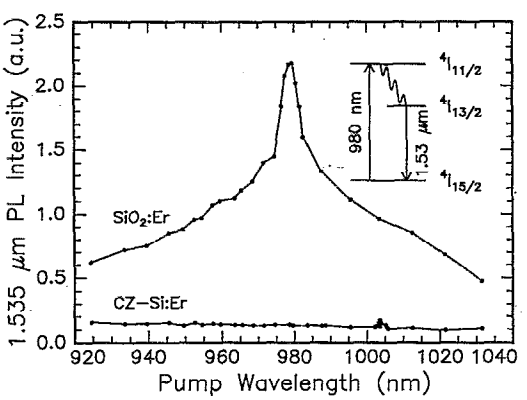

FIG. 3. Photoluminescence excitation spectrum of Er-implanted Cz-Si (250 keV, 9×10^{14} Er/cm^2+600 °C, 15 min+1000 °C, 15 s) at 77 K, and of an Er-implanted SiO_2 film (500 keV, 1.8×10^{15} Er/cm^2+900 °C, 30 min) at 77 K. The PL intensity at 1.535 μm is measured as a function of the pump wavelength. The pump power was 10 mW. The inset shows the Er energy-level diagram.

For comparison, a PL excitation spectrum of an Er-implanted SiO_2 film (500 keV, 1.7×10^{15} Er/cm^2, annealed at 900 °C) is also shown, measured using the same pump power of 10 mW. The peak in this spectrum corresponds to absorption at the $^4I_{15/2}\rightarrow{}^4I_{11/2}$ transition in Er^{3+}. After excitation to this level, the ion first decays nonradiatively to the $^4I_{13/2}$ level, whereupon it decays to the ground state by emission of a 1.535 μm photon (see inset in Fig. 3). From the fact that the peak at 980 nm is not observed in the spectrum for Er-doped Si, we conclude that the luminescence from Er in Si is due to a photocarrier-mediated process, rather than to direct absorption.

3. Discussion

Knowing that luminescent Er is excited electrically, the annealing characteristics in Fig. 2 may be explained. The fact that the Er PL lifetime increases from 0.75±0.05 to 0.98 ±0.05 ms indicates that the luminescence efficiency increases by 30% on annealing. The much larger (fivefold) increase in Er PL intensity upon annealing for 15 s must then result from either an increase in the optically active Er fraction or an increase in excitation efficiency. The increased BE PL intensity after 15 s annealing reflects an increased minority-carrier lifetime, attributed to annealing of carrier recombination centers remaining after SPE. Indeed, the defect band around 1.36 μm in the PL spectra of Fig. 1 has disappeared after annealing. As an increased carrier lifetime leads to a more efficient excitation of Er, we conclude that the fivefold increase in Er PL after 15 s annealing is mainly due to the increased carrier lifetime. The decrease in BE PL for longer annealing times may result from activation of chemical impurities introduced or activated in the Si in the RTA process, which reduce the carrier lifetime.

B. Maximum active Er concentration in Cz-Si

1. Er depth profiles

There have been some earlier studies on the concentration dependence of the Er luminescence in ion implanted Si.[3,4,6] In these studies Er was directly implanted into *c*-Si at a wide range of fluences. As is well established, defect structures in ion-implanted Si are very fluence dependent, ranging from isolated point defects to amorphous layers. Comparing Er luminescence intensities in materials with such a broad range of microstructures is obviously very difficult, even after annealing, since the minority-carrier lifetimes will depend on the implantation fluence. In this way, the carrier density available for excitation of Er is sample dependent, and Er PL intensities cannot be compared directly. We have circumvented these problems by first preamorphizing a Cz-Si surface layer with a 350 keV Si implant at 77 K, and then implanting 250 keV Er into the amorphous surface layer at fluences of 8×10^{11}, 8×10^{12}, 8×10^{13}, or 8×10^{14} Er/cm^2 (fluence, or areal density, is defined as the Er concentration in-

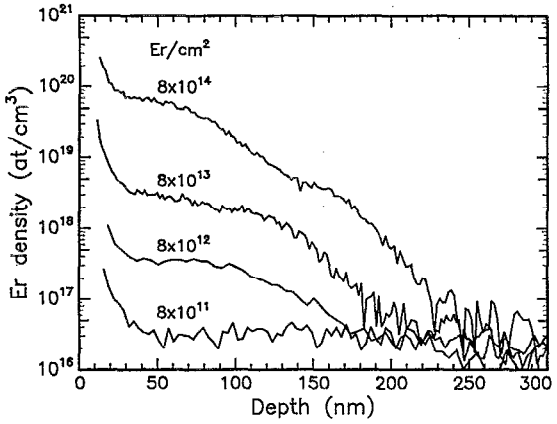

FIG. 4. SIMS Er depth profiles for four different samples. Cz-Si(100) was preamorphized using 350 keV Si, and then implanted with 250 keV Er at 8×10^{11}, 8×10^{12}, 8×10^{13}, and 8×10^{14} Er/cm^2. The samples were then recrystallized at 600 °C and subsequently annealed at 1000 °C for 15 s.

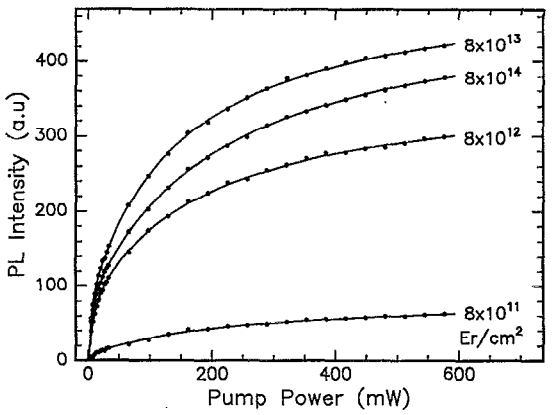

FIG. 5. Photoluminescence intensity at 1.54 μm as a function of pump power at 514.5 nm, measured at 77 K, for the samples in Fig. 4. The drawn lines are guides for the eye.

tegrated over the implanted depth). The Er-doped a-Si layers were then all recrystallized by SPE at 600 °C for 15 min and subsequently annealed at 1000 °C for 15 s.

Figure 4 shows SIMS measurements of the Er depth profiles for the four different samples after this treatment. The trapped Er concentrations range from 3×10^{16} to 7×10^{19} Er/cm^3. The profile for the lowest fluence (8×10^{11} Er/cm^2) is limited by the sensitivity of SIMS. The profiles for the two intermediate fluences are identical in shape, with the relative heights proportional to the implanted Er fluences. The shape of the profile for the highest Er fluence (8×10^{14} Er/cm^2) shows an enhanced trapped concentration between 30 and 100 nm depth, when compared to the shape for the samples with the lower concentrations. This is in agreement with our model of Er segregation and trapping at the moving amorphous-crystalline interface during SPE, in which it is postulated that defects in the amorphous Si near the moving interface act as traps for segregating Er.[18] According to this model, the relative amount of trapping in the crystal should increase when all traps on the amorphous side of the moving interface become filled at high Er concentrations, as is indeed observed in Fig. 4 for the highest fluence. All SIMS profiles show a peak near the surface corresponding to Er that has segregated out.

2. PL versus fluence

In Fig. 5, the Er PL peak intensity at 1.54 μm, measured at 77 K, is shown as a function of pump power for the four different samples. A rapid initial increase is seen for all samples, followed by a leveling off for higher pump powers. At a given pump power, the intensity increases with Er fluence for the three lowest fluences, and then decreases again for the sample implanted with 8×10^{14} Er/cm^2. The leveling off at high pump powers may be explained by the fact that a large fraction of Er becomes excited as the pump power (i.e., steady-state electrical carrier concentration) is increased. It is important to note that the shape of the four curves in Fig. 5 is identical, apart from a vertical scaling parameter which depends on the Er fluence. This implies that the recombination of electrical carriers is not dominated by the Er ions themselves, but rather by other structural defects of which the concentration is independent of Er concentration. The similarity in the shapes of the four curves in Fig. 5 implies that when comparing the PL intensity for different Er concentrations (Fig. 6), this comparison may be done at any pump power.

In Fig. 6 the PL intensity at 77 K, measured at a pump power of 160 mW, is plotted as a function of Er fluence for the four different samples. For the two low-fluence implants the PL intensity increases nearly linearly with fluence. Above 10^{13} Er/cm^2 the intensity levels off and does not increase much further. A small decrease in intensity is seen for the sample with 8×10^{14} Er/cm^2. Measurements of the Er PL lifetime as a function of Er fluence are also included in Fig. 6. The $1/e$ lifetime decreases with Er concentration, from 1.14 ± 0.05 ms for the lowest fluences to 0.74 ± 0.05 ms for

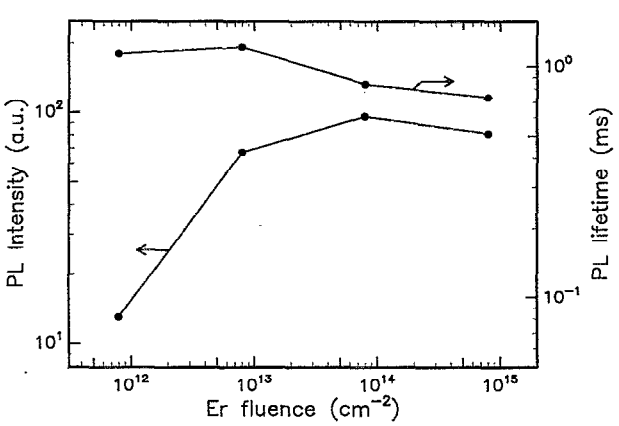

FIG. 6. Photoluminescence intensity and lifetime at 1.54 μm as a function of Er fluence, measured at 77 K, for the samples in Fig. 4. The pump power at 514.5 nm was 160 mW.

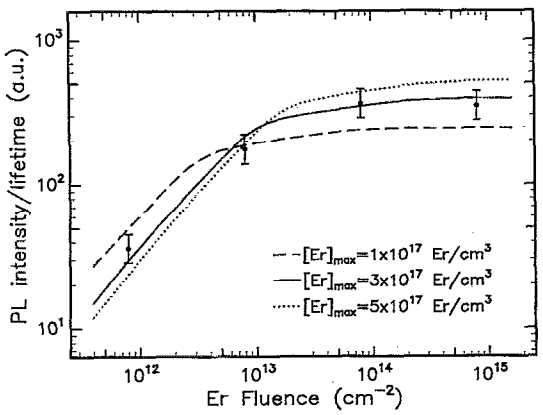

FIG. 7. Photoluminescence intensity divided by the lifetime (data from Fig. 6), which is a relative measure of the total areal density of optically active Er, plotted as a function of Er implantation fluence. The drawn lines are calculated from the SIMS profiles, using a model in which it was assumed that there is a maximum Er concentration that can be activated in Cz-Si. Curves are shown for $[Er]_{max}=1\times10^{17}$, 3×10^{17}, or 5×10^{17} Er/cm^3. The best agreement is obtained for $[Er]_{max}=(3\pm1)\times10^{17}$ Er/cm^3.

the highest fluence. The BE PL intensity was the same for all samples indicating that the minority-carrier lifetime was the same in each sample. Therefore, the carrier density available for excitation of Er was the same in all samples, enabling similar pump conditions for the Er. The fact that the minority-carrier density under steady-state pumping is similar for all Er concentrations again indicates that the Er ions themselves are not the dominant recombination centers for electrical carriers. This implies that only a small fraction of the photogenerated carriers is actually used to excite Er ions, and therefore the internal quantum efficiency for excitation is rather low.

Assuming that the Er PL lifetime is a measure for the luminescence efficiency, the PL intensity data can be corrected in order to obtain a relative measure of the optically active Er fluence. This is shown in Fig. 7, in which the PL intensity data from Fig. 6 are divided by the lifetime for each sample.

3. Concentration limit model

The data in Fig. 7 clearly show a saturation in optically active Er fluence above 10^{13} Er/cm^2. The data can be analyzed by assuming that there is a maximum Er concentration that can be optically activated $[Er]_{max}$. Any Er trapped at concentrations above $[Er]_{max}$ would then remain inactive. For each SIMS profile in Fig. 4 we can then determine the total areal density of optically active Er by calculating the integrated areal density of Er below $[Er]_{max}$. This areal density should then be proportional to the Er PL data in Fig. 7.

Two problems arise if this integration is done with the data in Fig. 4. First, it results in only four data points, rather than a continuous calculation as a function of fluence. Second, the data for the lowest fluence are inaccurate because of the SIMS sensitivity. To avoid these problems we have taken the SIMS profile for the 8×10^{13} Er/cm^2 implant as a representative depth profile, and scaled it with a factor proportional to the fluence, in order to model the Er profile for any fluence in the range 4×10^{11}–2×10^{15} Er/cm^2. For a certain value of $[Er]_{max}$ we then calculated for each fluence the integrated areal density of Er below $[Er]_{max}$. The continuous lines in Fig. 7 are results of this procedure, using three different values for $[Er]_{max}$. As the PL intensity is only measured in relative units, each curve was scaled in the vertical direction to obtain best agreement with the data. As can be seen, the best fit is obtained using $[Er]_{max}=(3\pm1)\times10^{17}$ Er/cm^3. This implies that, for example, for a 8×10^{14} Er/cm^2 implant (top curve in Fig. 4, with up to 7×10^{19} Er/cm^3 trapped in the crystal) only 6×10^{12} Er/cm^2, i.e., less than 1% of the implanted fluence, is optically active.

C. Er configuration in Si

Previous experiments have shown that the addition of oxygen to Er-implanted Cz-Si can enhance the Er PL intensity.[3,4,9] The addition of O increases the luminescent Er concentration and reduces the PL quenching at elevated temperatures.[19] Extended x-ray-absorption-edge fine-structure spectroscopy (EXAFS) measurements have shown that Er forms clusters with O. It was concluded that Er in this cluster was coordinated by roughly 4–6 O atoms.[14]

Using this coordination number and the known O content in our Cz wafer of $(1.7\pm0.5)\times10^{18}$ O/cm^3, and assuming that in the Er-doped region all Er is bound to oxygen, we can derive a separate estimate of $[Er]_{max}$: 2–6×10^{17} Er/cm^3. This number is in good agreement with the number found above from Fig. 7. As these Er-O complex seem to form so readily, we can consider Er as a microscopic getter in Si which binds with any O within a typical diffusion distance. This then has an important consequence for the definition of the solubility of Er in Si. By analogy with the transition metals the solubility of Er in pure single-crystal Si would likely be relatively low (10^{14}–10^{16} Er/cm^3).[29] Other measurements[11] have suggested that the solubility in Cz-Si is around 1×10^{18} Er/cm^3. Given the strong tendency for Er to bind with O, we suggest that in Cz-Si with $(1.7\pm0.5)\times10^{18}$ O/cm^3, oxygen enhances the effective solubility of Er to at least $[Er]_{max}=3\times10^{17}$ Er/cm^3, i.e., no Er-related precipitates will be observed up to this Er concentration in Cz-Si. Indeed, this is in agreement with transmission electron microscopy data.[11,13] Also, this solubility model explains the observation that if high Er and O concentrations are co-implanted in such a ratio that not enough O is available to bind all Er in Er-O clusters, Er-related precipitates are formed.[9] From the annealing studies in Fig. 2 it follows that the Er-O clusters are stable up to at least 1000 °C.

It is interesting to compare our data on the optical activation of Er in Cz-Si with those on electrical activation. Er exhibits donor behavior in Si and it was found[7] that the maximum carrier concentration in Cz-Si was reached for an Er concentration of $(4$–$7)\times10^{17}$ Er/cm^3, very similar to the value found in the present article for optical activation. These data suggest that the optically and electrically active Er sites in Si may be the same. Such a correlation between optically and electrically active sites also follows from O codoping experiments which showed that O enhances both the optically and electrically active fraction.[7,9]

More measurements will be required to determine the nature of the large optically (and electrically) inactive fraction of Er in Cz-Si. Preliminary x-ray-absorption spectroscopy measurements on samples in which only 1 at. % Er is optically active, show that all Er is in the trivalent charge state.[30] This suggests that the inactive Er has either a very small luminescence quantum efficiency (short luminescence lifetime) or a small excitation efficiency, and therefore does not contribute to the PL spectra.

D. Quantum efficiency

Using the data in Fig. 3 we can make a rough estimate of the internal quantum efficiency for carrier-mediated excitation of Er in Si. We compare the PL intensities for the Er-doped Si and SiO_2 samples, at a pump wavelength of 980 nm. At this wavelength, the absorption cross section σ_a for optical absorption of Er in SiO_2 is known and the PL intensity from Er in SiO_2 is given by

$$I_{\text{opt}}=\frac{I_{\text{pump}}}{h\nu_{\text{pump}}}\sigma_a\phi_0 c_0, \tag{1}$$

with I_{pump} the pump intensity, h Planck's constant, υ_{pump} the pump frequency, ϕ_0 the Er fluence in the oxide, and c_0 a correction factor taking into account reflection and refraction of the pump beam as well as the collection efficiency. For electrical excitation of Er in Si we can write for the PL intensity

$$I_{\text{el}}=\frac{I_{\text{pump}}}{h\nu_{\text{pump}}}Qc_s, \tag{2}$$

with Q the quantum efficiency, defined as the fraction of photogenerated electron-hole pairs that recombine by transferring energy to an Er ion, and c_s the correction factor for Si. Combining Eqs. (1) and (2) we find

$$\frac{I_{\text{el}}}{I_{\text{opt}}}=\frac{c_sQ}{c_0\sigma_a\phi_0}. \tag{3}$$

From Fig. 3 we determine the ratio $I_{\text{el}}/I_{\text{opt}}=0.06$. Using a recent measurement of σ_a (2×10^{-21} cm^2),[31] the known fluence ϕ_0, and estimates for c, we can solve the only unknown parameter $Q=3\times10^{-6}$. Note that this calculation assumes that all photogenerated carriers recombine in the Er-doped region. In reality, a significant fraction of the carriers will recombine outside this region. The number of 3×10^{-6} is, therefore, a lower limit.

This value for the quantum efficiency is a small number, and indicates that the main carrier recombination route is not through Er ions. This follows also implicitly from the observation that all samples in Fig. 6, with a large range of Er concentrations, had the same band-edge luminescence and, therefore, carrier lifetime. It also follows from the fact that the pump power dependence in Fig. 5 is the same for all Er concentrations. Clearly, the structural defects remaining after SPE, such as for example end-of-range dislocations, dominate the electrical characteristics in these samples. Future work should focus on reduction or passivation of these defects. The quantum efficiency can be further increased if the Er active fraction is increased. By co-implanting additional oxygen, and by increasing the Er depth using MeV implantation energies, we expect that the quantum efficiency can be improved to 10^{-2}–10^{-3}.

IV. CONCLUSION

In conclusion, we have addressed several requirements for the attainment of efficient luminescence of Er in Si, as follows.

(1) High Er concentrations, up to 7×10^{19} Er/cm^3, were incorporated by SPE crystallization of an implantation-amorphized Er-doped Si surface layer at 600 °C.
(2) A fraction of the Er is optically active after SPE and the photoluminescence intensity at 1.54 μm can be further optimized by subsequent thermal annealing at 1000 °C for 15 s. In Cz-grown Si the optically active Er concentration is limited to $(3\pm1)\times10^{17}$ Er/cm^3.
(3) The luminescence lifetime at 77 K is around 1 ms. This is in the same order of magnitude as the radiative lifetime of Er in many solids, and therefore the luminescence efficiency at 77 K is high. Due to strong temperature quenching, no luminescence is observed at room temperature; However, as we have shown in previous work[19] the quenching can be reduced by the addition of impurities, such as oxygen.
(4) Er is excited through photocarriers, and therefore the photocarrier lifetime is an important parameter determining the luminescence intensity. This should be taken into account when impurities are co-implanted to enhance the active Er concentration, as such impurities and the structural defects associated with their incorporation will decrease the minority-carrier lifetime. The internal quantum efficiency for excitation of Er is larger than 3×10^{-6}, and can be improved by increasing the optically active Er concentration, for example by co-implantation of oxygen and distribution of the Er over larger depths.

ACKNOWLEDGMENTS

This work is part of the research program of the Foundation for Fundamental Research on Matter (FOM) and was made possible by financial support from the Dutch Organization for the Advancement of Pure Research (NWO), the Netherlands Technology Foundation (STW), and the IC Technology Program (IOP Electro-Optics) of the Ministry of Economic Affairs. R.S. acknowledges financial support from CSIC, Spain.

[1] H. Ennen, J. Schneider, G. Pomrenke, and A. Axmann, Appl. Phys. Lett. **43**, 943 (1983).
[2] H. Ennen, G. Pomrenke, A. Axman, K. Eisele, W. Haydl, and J. Schneider, Appl. Phys. Lett. **46**, 381 (1985).
[3] P. N. Favennec, H. l'Haridon, D. Moutonnet, M. Salvi, and M. Gauneau, Jpn. J. Appl. Phys. **29**, L524 (1990).
[4] J. Michel, J. L. Benton, R. F. Ferrante, D. C. Jacobson, D. J. Eaglesham, E. A. Fitzgerald, Y.-H. Xie, J. M. Poate, and L. C. Kimerling, J. Appl. Phys. **70**, 2672 (1991).
[5] Y. S. Tang, K. C. Heasman, W. P. Gillin, and B. J. Sealy, Appl. Phys. Lett. **55**, 432 (1989).
[6] D. Moutonnet, H. l'Haridon, P. N. Favennec, M. Sali, M. Gauneau, F. Arnaud d'Avitaya, and J. Chroboczek, Mater. Sci. Eng. B **4**, 75 (1989).
[7] J. L. Benton, J. Michel, L. C. Kimerling, D. C. Jacobson, Y. -H. Xie, D. J.

Eaglesham, E. A. Fitzgerald, and J. M. Poate, J. Appl. Phys. **70**, 2667 (1991).
[8] F. P. Widdershoven and J. P. M. Naus, Mater. Sci. Eng. B **4**, 71 (1989).
[9] F. Priolo, S. Coffa, G. Franzó, C. Spinella, A. Carnera, and V. Bellani, J. Appl. Phys. **74**, 4936 (1993).
[10] W. P. Gillin, J.-P. Zhang, and B. J. Sealy, Solid State Commun. **77**, 907 (1991).
[11] D. J. Eaglesham, J. Michel, E. A. Fitzgerald, D. C. Jacobson, J. M. Poate, J. L. Benton, A. Polman, Y.-H. Xie, and L. C. Kimerling, Appl. Phys. Lett. **58**, 2797 (1991).
[12] A. Polman, J. S. Custer, E. Snoeks, and G. N. van den Hoven, Nucl. Instrum. Methods B **80/81**, 653 (1993).
[13] A. Polman, J. S. Custer, E. Snoeks, and G. N. van den Hoven, Appl. Phys. Lett. **62**, 507 (1993).
[14] D. L. Adler, D. C. Jacobson, D. J. Eaglesham, M. A. Marcus, J. L. Benton, J. M. Poate, and P. H. Citrin, Appl. Phys. Lett. **61**, 2181 (1992).
[15] J. S. Custer, A. Polman, E. Snoeks, and G. N. van den Hoven, Mater. Res. Soc. Proc. **301**, 101 (1993).
[16] M. Efeoglu *et al.* Semicond. Sci. Technol. **8**, 238 (1993).
[17] Y. S. Tang, J.-P. Zhang, K. C. Heasman, and B. J. Sealy, Solid State Commun. **72**, 991 (1989).
[18] J. S. Custer, A. Polman, and H. M. van Pinxteren, J. Appl. Phys. **75**, 2809 (1994).
[19] S. Coffa, G. Franzò, F. Priolo, A. Polman, and R. Serna, Phys. Rev. B **49**, 16 313 (1994).
[20] S. Lombardo, S. U. Campisano, G. N. van den Hoven, A. Cacciato, and A. Polman, Appl. Phys. Lett. **63**, 1942 (1993).
[21] G. N. van den Hoven, A. Polman, S. Lombardo, and S. U. Campisano (unpublished).
[22] R. Serna, E. Snoeks, G. N. van den Hoven, and A. Polman, J. Appl. Phys. **75**, 2644 (1994).
[23] F. Y. G. Ren, J. Michel, Q. Sun-Paduano, B. Zheng, H. Kitagawa, D. C. Jacobson, J. M. Poate, and L. C. Kimerling, Mater. Res. Soc. Proc. **301**, 87 (1993).
[24] G. Franzò, F. Priolo, S. Coffa, A. Polman, and A. Carnera, Appl. Phys. Lett. **64**, 2235 (1994).
[25] S. Lombardo, S. U. Campisano, G. N. van den Hoven, and A. Polman (unpublished).
[26] R. G. Wilson, F. A. Stevie, and C. W. Magee, *Secondary Ion Mass Spectrometry* (Wiley, New York, 1989).
[27] G. E. Jellison and F. A. Modine, J. Appl. Phys. **53**, 3745 (1982).
[28] G. Davies, Phys. Rep. **176**, 83 (1989).
[29] F. A. Trumbore, Bell Syst. Tech. J. **39**, 205 (1960).
[30] J. B. Goedkoop and A. Polman (unpublished).
[31] G. N. van den Hoven and A. Polman (unpublished).